Guo *et al. Bioresources and Bioprocessing* (2026) 13:60
https://doi.org/10.1186/s40643-026-01064-x

Bioresources
and Bioprocessing

RESEARCH Open Access

Long-root *Eichhornia crassipes* waste plants dual-purpose resource utilization: green preparation of magnetic carbon quantum dots for heavy metal deep removal

Yihong Guo[1,2], Mingxin Cui[1*], Hongjun Yang[3], Jun Chen[2*] and Sen Lin[1,2*]

Abstract

Long-root *Eichhornia crassipes*, an aquatic plant with extensive root systems, has demonstrated potential in remediating eutrophicated water bodies. However, improper disposal of large quantities of discarded plants post-remediation can easily cause secondary pollution. In this study, rapidly recoverable magnetic carbon quantum dots (MCQDs) were greenly synthesized via hydrothermal treatment of long-root *Eichhornia crassipes* and subsequent coupling with Fe_3O_4 nanoparticles. Adsorption experiments demonstrated that MCQDs displayed a commendable adsorption capacity for various heavy metals in municipal wastewater under the synergistic effect of CODs and Fe_3O_4. Mechanistic analyses revealed that the adsorption involved chemical binding with oxygen-containing functional groups and amino groups on the surface of MCOQs. The saturated MCQDs were efficiently recovered within 5 min using an applied magnetic field, offering a practical solution for nanoparticle recovery. This study provides valuable insights into the green resource utilization of Long-root *Eichhornia crassipes* based on CQD technology.

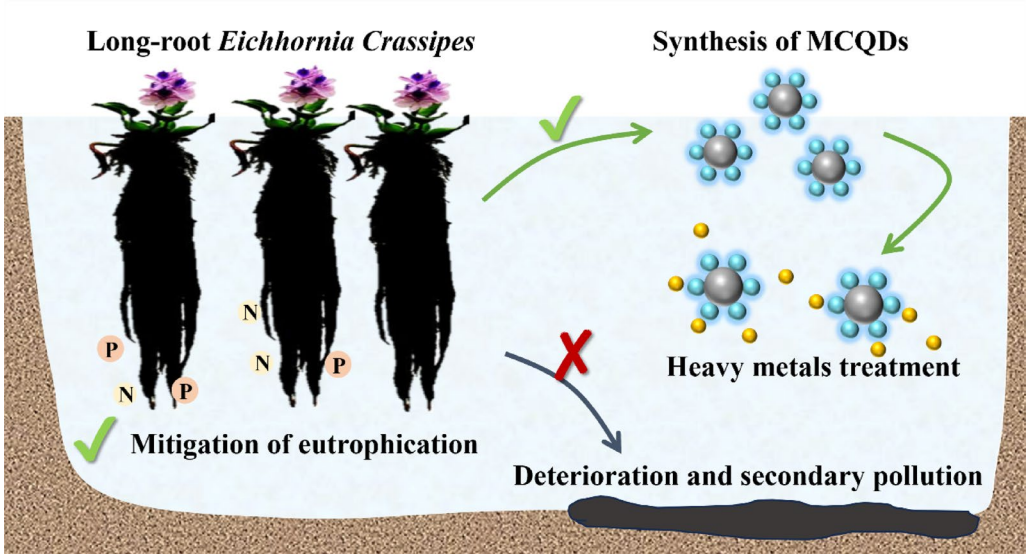
Keywords Adsorption, Carbon quantum dots, Heavy metals, Long-root *Eichhornia crassipes*, Magnetic nanopartion

*Correspondence:
Mingxin Cui
2013990005@qhu.edu.cn
Jun Chen
chenjun2024@ecust.edu.cn
Sen Lin
linsen@ecust.edu.cn

Full list of author information is available at the end of the article

© The Author(s) 2026. **Open Access** This article is licensed under a Creative Commons Attribution 4.0 International License, which permits use, sharing, adaptation, distribution and reproduction in any medium or format, as long as you give appropriate credit to the original author(s) and the source, provide a link to the Creative Commons licence, and indicate if changes were made. The images or other third party material in this article are included in the article's Creative Commons licence, unless indicated otherwise in a credit line to the material. If material is not included in the article's Creative Commons licence and your intended use is not permitted by statutory regulation or exceeds the permitted use, you will need to obtain permission directly from the copyright holder. To view a copy of this licence, visit http://creativecommons.org/licenses/by/4.0/.

Graphical abstract



Introduction

Long-root *Eichhornia crassipes* is a recently developed variety of water hyacinth employed to mitigate eutrophication of aquatic ecosystems (Lin et al. 2018; Liu et al. 2021). Compared with traditional plants, it has a more developed root system, accounting for more than 80%, and an excellent ability to remove nitrogen and phosphorus to limit the malicious spread of algae in the water (Liu et al. 2018). However, the harvested plants after wastewater treatment often accumulate in large quantities, leading to secondary pollution and disposal challenges if not properly managed. Consequently, how to deal with waste plant and recycle it as a usable resource is a pressing challenge (Lin et al. 2012, 2022). Due to its well-developed root system and low moisture content, current research focuses on its application in the preparation of activated carbon or other modified adsorbents (Cao et al. 2019; Lin et al. 2020). Converting waste biomass into functional nanomaterials offers a promising solution that addresses both waste disposal and pollution remediation.

Carbon quantum dots (CQDs), less than 10 nm in diameter, have abundant functional groups on surface, good fluorescence characteristics, biocompatibility, and non-toxicity, enabling their wide application in environmental, biomedical, bioenergy, and food safety fields (Wang and Hu 2014; Chen et al. 2021a, b, c; Luo et al. 2021). Preparation methods of CQDs can be divided into the "Top-down" method that converts bulk carbon materials into nanoparticles by oxidation, reduction, stripping and shearing, and "Bottom-up" approaches that fuse or carbonize small molecular compounds by high-temperature pyrolysis and spontaneous chemical reactions (Tian et al. 2009; Yang et al. 2009; Bao et al. 2011). However, existing methods for CQDs synthesis often involve difficult reaction conditions, high costs, cumbersome processes, and toxic raw materials, limiting their scalable preparation and practical application.

The usage of green and natural substances as synthetic raw materials may overcome these disadvantages and be additionally valuable (Mahesh et al. 2016; Jia et al. 2024). As a green and biocompatible nanomaterial, carbon quantum dots derived from diverse carbohydrate sources have shown great potential for broad applications across environmental, biomedical, and food safety fields (Berdimurodov et al. 2025). Selecting the roots of waste Long-root *Eichhornia crassipes* plants as raw material not only enables environmentally friendly CQDs production but also offers a sustainable solution for repurposing waste biomass reuse and heavy metals pollution treatment.

In this work, CQDs generated by waste Long-root *Eichhornia crassipes* plants can be uniformly doped with superparamagnetic nanoparticles (Fe_3O_4 or γ-Fe_2O_3) to create hybrid magnetic CQDs (MCQDs), which can be used for heavy metal removal in the water bodies. The physicochemical properties of MCQDs were comprehensively characterized, and their magnetic recovery behavior was investigated through kinetics measurement. Moreover, the adsorption performance was evaluated through kinetics and thermodynamic experiments, based on which the mechanism of efficient heavy metal adsorption by MCQDs was determined. This work demonstrated a sustainable strategy wherein waste Long-root *Eichhornia crassipes* biomass, originally employed for ammonia nitrogen removal, is repurposed as a precursor

for magnetic carbon quantum dots for heavy metal remediation, achieving dual-purpose benefits in both ammonia nitrogen pollution treatment and heavy metal remediation.

Experimental sections

Materials and reagents

All metal salt chemicals were purchased from Macklin Biochemical Technology Co., Ltd. Ammonium nitrate and sodium hydroxide were bought from Sinopharm Chemical Reagent Co., Ltd. All chemicals used in this study were of analytical reagent grade.

Synthesis of Fe_3O_4

The synthesis was conducted in a jacketed reactor with a water bath temperature of 45 °C and a stirring rate of 300 rpm. 2.7062 g $FeCl_3$ $6H_2O$ and 0.9954 g $FeCl_2$ $4H_2O$ were dissolved in 100 mL of deionized water under stirring. After complete dissolution, 6 mL of NaOH solution (8 mol/L) was rapidly added. The mixture was stirred for 30 min, yielding a Fe_3O_4 suspension.

Synthesis of MCQDs

Based on literature review and preliminary experiments on biomass-derived CQDs (Nguyen et al. 2022; Durairaj et al. 2022; Kunnath Parambil et al. 2025), CQDs were successfully synthesized via hydrothermal reaction of long-root *Eichhornia crassipes* root powder in deionized water at 180 °C for 10 h. The products were centrifuged (10000 rpm, 20 min) to obtain the CQDs liquid. Subsequently, the CQDs solution was thoroughly combined with a Fe_3O_4 suspension prepared by co-precipitation of a Fe (III)/Fe (II) mixture in a NaOH solution to obtain MCQDs.

Adsorption kinetics

All adsorption kinetics experiments in this work were conducted at 30 °C, with the mass ratio of MCQDs adsorbent to heavy metal solution meticulously maintained at 0.5 g per 150 mL. Samples were collected at appropriate intervals and analyzed to determine the concentration of heavy metal ions. The adsorption capacity q_e (mmol/g) was calculated according to Eq. (1)

$$q_e = \frac{(C_0 - C_t)\,V}{m} \tag{1}$$

where C_0 and C_t were the beginning and residual concentrations (mmol/L) of heavy metal in solution, respectively, V was the adsorption solution volume (L), and m was the mass of MCQDs (g).

Adsorption isotherm

Adsorption isotherm measurements were carried out at 15, 30, and 50 °C using heavy metal solutions with initial concentrations ranging from 0 to 1 mmol/L. The duration of experiments was set at 10 h to ensure that the adsorption process reached equilibrium.

Magnetic recovery

For the magnetic recovery experiments, three samples were prepared by dispersing 0.1, 0.2, and 0.3 g of MCQDs particles in 100 mL of solution, respectively. Each suspension was placed under a static magnetic field generated by a 0.1 T permanent magnet for 5 min. The magnetic recovery was determined by measuring the iron element of unrecovered MCQDs in the suspension. The magnetic recovery ratio η was calculated according to Eq. (2).

$$\eta = \left(1 - \frac{c_t}{c_0}\right) \times 100\% \tag{2}$$

where c_t was the Fe^{3+} concentration of the sample with unrecovered suspended MCQDs particles that were collected and dissolved at specified times, and c_0 was the initial Fe^{3+} concentration of the uniform suspension.

Assays

The photoluminescence (PL) spectra were recorded using a fluorescence spectrophotometer (LS-55, PerkinElmer, America). The surface situation of MCQDs was observed utilizing a scanning electron microscope (SEM, GeminiSEM 360, ZEISS, Germany). To further analysis of MCQDs, TEM images were acquired by the transmission electron microscope (Talos F200x, Thermo Fisher, America). Particle size analysis of MCQDs was performed using a laser particle size analyzer (Mastersizer 3000, Malvern, UK). Deionized water was used as the dispersant, and the obscuration level was controlled within 10–15% during the measurement. X-ray photoelectron spectra (XPS) of surface elements were obtained through the X-ray analyzer (Nexsa, Thermo Fisher, America) with greater than 3 μm of resolution. The pattern of MCQDs was obtained by X-ray diffractometer (XRD, SmartLab SE, Rigaku, Japan) with a scanning range of 5°-80°. Fourier transform infrared spectra were determined with an FT-IR spectrometer (Nicolet iS20, Thermo Fisher, America). The magnetic performance was tested on a vibrating sample magnetometer (7404, LakeShore, America). The thermal gravimetric analyzer (TGA, SDTQ600, TA, America) was conducted to measure the weight loss of MCQDs and Fe_3O_4 within the temperature range of 10–600 °C. The surface area and pore size distributions results of MCQDs were obtained by BET instrument (ASAP 2460, Micromertics, America). The metal ions

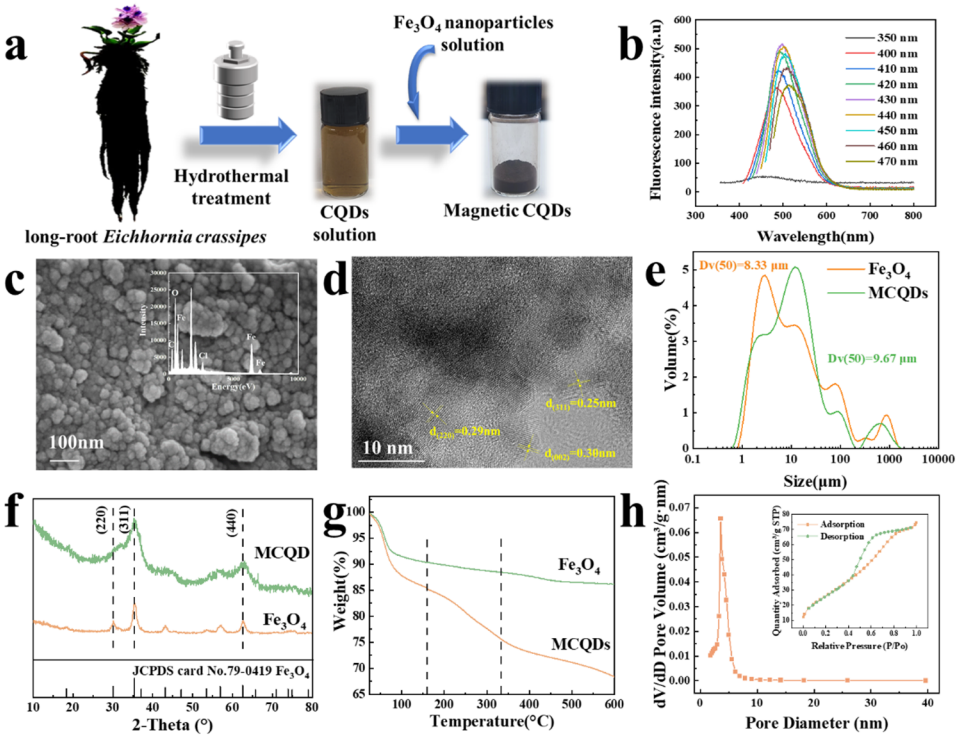


Fig. 1 Synthetic schematic of MCQDs (**a**). The PL spectra of CQDs liquid (**b**). The surface morphology (**c**), HRTEM image (**d**), particle size distribution (**e**), XRD patterns (**f**), TG results (**g**), and N_2 adsorption/desorption isotherms (measured at 77 K) (**h**) of MCQDs

concentrations were determined by an ICP-OES instrument (ARCOS, Spectro, Germany).

Results and discussion

MCQDs characterization

As shown in Fig. 1a, a CQDs solution was prepared using long-root *Eichhornia crassipes* root powder and combined with magnetic substances to form magnetic CQDs. It could be seen in Fig. 1b that the CQDs solution exhibited photoluminescence behavior, with maximum emission at 500 nm under 430 nm excitation, confirming the successful preparation of the CQDs solution (Zhu et al. 2013). SEM images were shown in Fig. 1c. The MCQDs nanoparticles had a granular structure, but the particles were mostly clustered together with a wide range of particle size distributions due to the presence of Fe_3O_4 magnetism. Figure 1d showed the HRTEM images of MCQDs. The spacing of 0.25 and 0.29 nm, respectively, was found to be consistent with Fe_3O_4 (Chen et al. 2021a, b, c). The graphitic carbon with a lattice spacing of about 0.30 nm was at flanks of Fe_3O_4 particles (Đorđević 2022). The elemental mappings were shown in Fig. S1, and the distribution of the elements was uniform and dense. The above results certified the good distribution of CQDs on Fe_3O_4.

Laser particle size analysis showed that bare Fe_3O_4 had a median particle size of 8.33 μm, while MCQDs had a median particle size of 9.67 μm, indicating that the co-precipitation process did not significantly alter the Fe_3O_4 particle size (Fig. 1e). It is well documented that Fe_3O_4 nanoparticles prepared by co-precipitation tend to form aggregates in solution while their primary particles remain in the nanoscale range (Abboud et al. 2015). As shown in Fig. 1f, the obvious characteristic peaks were consistent with Fe_3O_4 (JCPDS card No. 79-0419), confirming that the synthesis of Fe_3O_4 could be achieved through this methodology. However, due to the low CQDs content in the composite adsorbent, the characteristic peak of graphite was absent in the MCQDs. XRD analysis showed that the diffraction peaks of Fe_3O_4 in MCQDs became slightly broader compared to bare Fe_3O_4, which may indicate reduced crystallinity due to the interaction with CQDs. These results were consistent with our previous studies on magnetic materials, where functionalization of Fe_3O_4 typically does not alter their core structure (Lin et al. 2018; Chen et al. 2020, 2021a, b, c). The XRD results agreed with the emergency of the characteristic peaks in XPS spectra (Fig. S2a), which verified the well combination of Fe_3O_4 and CQDs in the MCQDs. The FT-IR spectra of the Fe_3O_4 and MCQDs were shown in Fig. S2b. After linking with CQDs, a new peak was observed at 1097 cm^{-1}, which belonged to the alkoxy peak and at 2920 cm^{-1} showed the stretching vibration of C-H in the spectrum (Wang et al. 2016). The abundance of hydroxyl groups on the surface of MCQDs made the adsorbent well-hydrophilic. The MCQDs

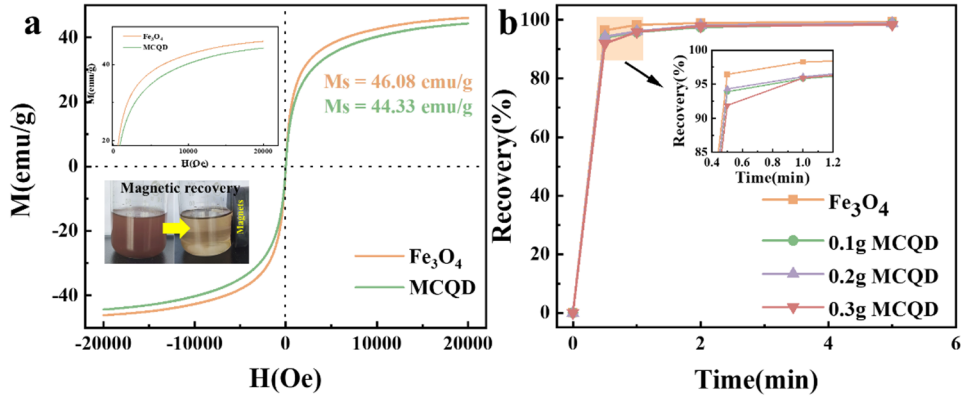


Fig. 2 Magnetic hysteresis loops of MCQDs and bare Fe_3O_4 (**a**). The magnetic recovery kinetics of MCQDs and bare Fe_3O_4 (**b**)

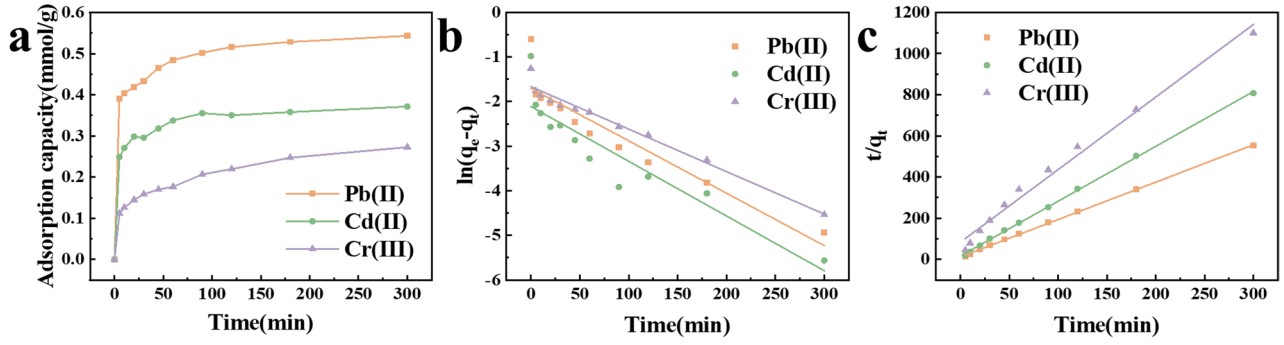


Fig. 3 Adsorption kinetics of heavy metals on MCQDs (**a**), and fitting lines of pseudo-first-order model (**b**) and pseudo-second-order model (**c**)

exhibited a slight shift in the characteristic Fe-O vibration peak compared with bare Fe_3O_4, indicating interaction between Fe_3O_4 and CQDs, which was consistent with literature reports (Mashkani et al. 2018; El Ghacham et al. 2025).

Thermogravimetry allowed further investigation of the thermal properties and composition of the nanocomposites (Fig. 1g). The thermal evolution of the MCQDs included three stages. A weight loss occurred at the first stage, attributed to evaporation of hydrogen-bonded water. Subsequently, mass loss occurred at the second stage. Additionally, weight loss was observed at the last stage, indicating combustion of the carbon skeleton in the CQDs. TG analyses indicated the successful binding of CQDs to Fe_3O_4.

Meanwhile, the pore structures of MCQDs were studied to investigate specific surface areas by BET analysis (Fig. 1h). The pore size of MCQDs was predominantly 3–5 nm, with a majority of micropores and mesopores. The adsorption isotherms of MCQDs all belonged to type IV isotherms, suggesting the occurrence of capillary condensation within the mesopores. The hysteresis loops observed were of the H2 type, which indicated a complex pore structure. Furthermore, the internal structure and surface characteristics of MCQDs revealed specific surface area was 98.25 m^2/g, and the average pore size was 4.70 nm, which could facilitate fast mass diffusion.

Magnetic recovery process

Figure 2a showed that the magnetic hysteresis loops of MCQDs and Fe_3O_4 were both S-shaped curves, illustrating the superparamagnetism of MCQDs (Chen et al. 2012). The saturation magnetization (Ms) of MCQDs was 44.33 emu/g, which was less than Fe_3O_4 nanoparticle, which theoretically ensured that MCQDs can be demagnetized and dispersed in solution quickly after removal of the magnetic field. Magnetic recovery experiments showed that the aggregation of particles was quite slow by gravity alone, however, magnetic particles gathered rapidly in one direction upon application of a magnetic field. Once the external field was removed, the dispersion was quickly re-established by stirring slightly. Figure 2b showed the recovery efficiency of MCQDs with different contents in the presence of an external magnetic field. The trend of the recovery of suspensions with different concentrations was consistent, and the recovery efficiency was close to 100% after 5 min, illustrating the complete separation of MCQDs in solution via magnetic force in a short time, and the recovery rate was almost independent of the content of MCQDs.

Table 1 The parameters of the fitted kinetic data

		Pb (II)	Cd (II)	Cr (III)
Pseudo-first-order kinetic model	q_e (mmol/g)	0.1820	0.1210	0.1893
	k_1 (min^{-1})	0.0118	0.0123	0.0095
	R^2	0.8647	0.8375	0.9689
Pseudo-second-order kinetic model	q_e (mmol/g)	0.5505	0.3753	0.2836
	k_2 (g/(mmol min))	0.2809	0.4459	0.1495
	R^2	0.9993	0.9993	0.9861

Table 2 Adsorption isotherm and thermodynamics parameters for adsorption

		15 °C	30 °C	50 °C
Langmuir	q_m (mmol/g)	0.33	0.35	0.39
	K_L (L/mmol)	44.2009	48.7086	100.3626
	R^2	0.4982	0.6634	0.8347
Freundlich	K_F [mmol/g (mmol/L)$^{-1/n}$]	0.3433	0.3556	0.4049
	1/n	0.1236	0.1180	0.0770
	R^2	0.8772	0.9595	0.9902
Thermo-dynamic parameters	ΔG^0 (kJ/mol)	-19.37	-21.35	-34.88
	ΔH^0 (kJ/mol)		110.55	
	ΔS^0 (J/mol K)		445.54	

Adsorption kinetics

The tendency of heavy metal adsorption capacity of MCQDs with time was shown in Fig. 3a. The adsorption kinetic curves of different metal ions were the same, and the metals adsorption equilibrium was reached after 3 h. For further understanding of the adsorption process and optimization of the adsorption conditions, the fitting of the heavy metal adsorption process to MCQDs was determined by the pseudo-first-order model (Eq. 3) and the pseudo-second-order model (Eq. 4), respectively (Bilgili 2006; Cheung et al. 2007).

$$\ln\left(q_e - q_t\right) = \ln q_e - k_1 t \tag{3}$$

$$\frac{\mathrm{t}}{\mathrm{q_t}} = \frac{1}{\mathrm{k_2 q_e^2}} + \frac{\mathrm{t}}{\mathrm{q_e}} \tag{4}$$

where q_e (mmol/g) was the adsorption capacity at final time; q_t (mmol/g) was capacity at specific time; k_1 (min^{-1}) and k_2 (g/(mmol·min)) were the rate constant of models, respectively.

The kinetic fitting lines and the fitted kinetic data were presented in Fig. 3b–c; Table 1. The correlation of the pseudo-second-order equation was significantly better than the other one, which indicated the adsorption process can be explained by the pseudo-second-order kinetic model, which explains that the adsorption process was controlled by chemisorption.

Adsorption isotherms

By varying the concentration of heavy metal ions, the relationships between the equilibrium adsorption capacity of Cd (II) by MCQDs and the equilibrium concentration at three temperatures were measured and were shown in Fig. 4a–c. The Freundlich equation exhibited a slightly higher degree of fit than the Langmuir equation. The parameters and correlation coefficients were listed in Table 2. Furthermore, the standard thermodynamic analysis for the adsorption of Cd (II) on MCQDs were calculated by Eqa. (5)–(7) (Lima et al. 2019). As shown in the results in Table 2, the ΔG^0 value was smaller than zero, indicating that the spontaneous adsorption process of MCQDs can be proved by higher temperature. The positive ΔH^0 values indicated the endothermic nature of the process, while the positive ΔS^0 value suggested an increase in disorder at the solid-solution interface.

$$\Delta G^0 = -nRT \tag{5}$$

$$\Delta G^0 = -RT \ln K \tag{6}$$

$$\ln K = \frac{\Delta S^0}{R} - \frac{\Delta H^0}{RT} \tag{7}$$

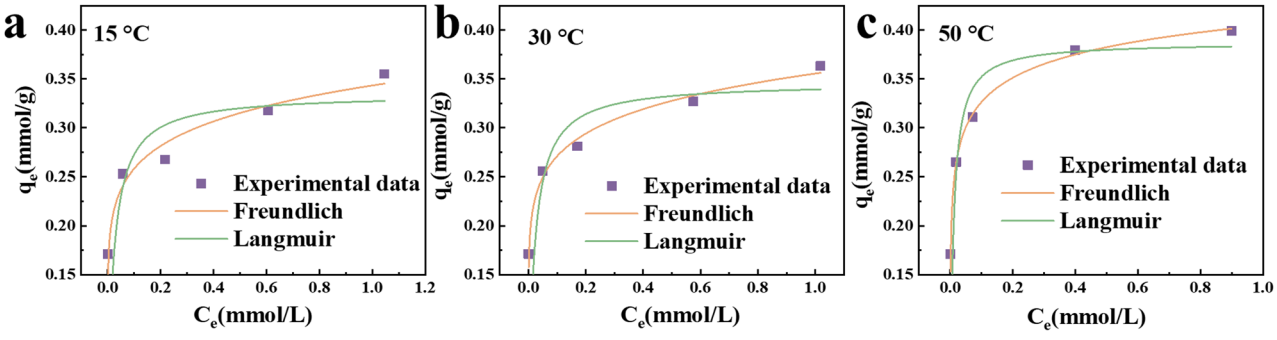


Fig. 4 Adsorption isotherms for Cd (II) onto MCQDs at 15 °C (**a**), 30 °C (**b**), and 50 °C (**c**) fitted with Langmuir and Freundlich models

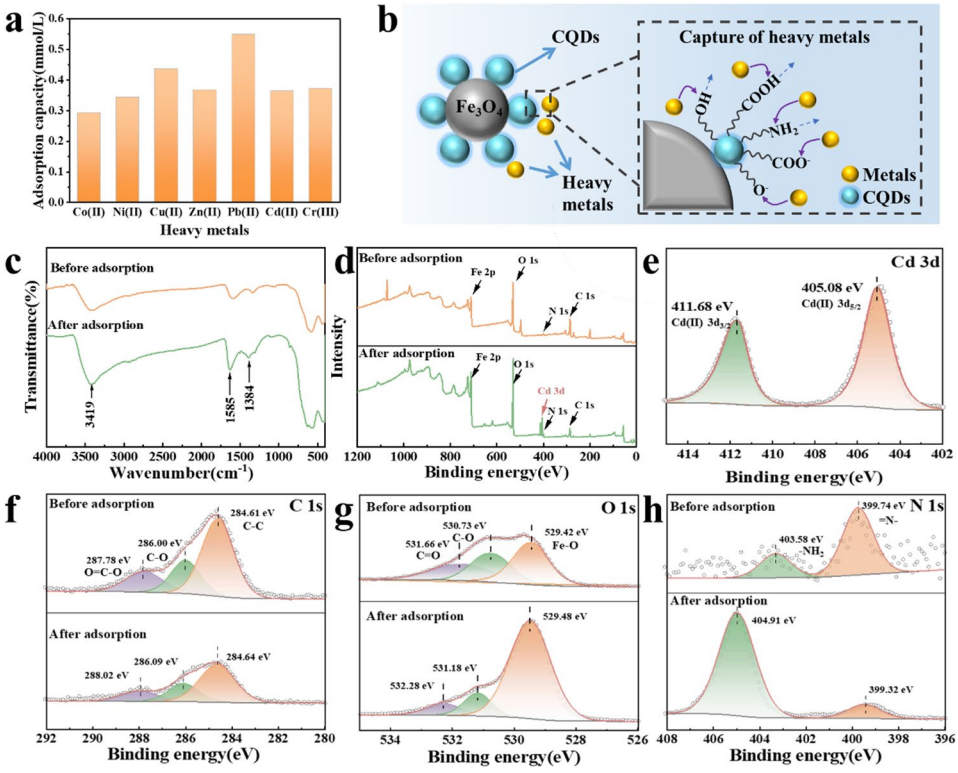


Fig. 5 The adsorption performance for different heavy metals (a). The schematic of adsorption mechanism of MCQDs (b). The FT-IR spectra (c) and XPS full spectra (d) of MCQDs before and after Cd (II) adsorption. The XPS spectra of Cd 3d(e), C 1s (f), O 1s (g), and N 1s (h) of MCQDs before and after Cd (II) adsorption.

Table 3 Summary of adsorption capacities of different magnetic CQDs materials

Adsorbent	Heavy metals	Adsorption capacity (mmol/g)	References
Fe_3O_4-PPCQDs	Cd (II)	0.1594	Pourshojaei et al. 2021
	Pb (II)	0.1146	
GSCQD-$FeFe_2O_4$	Pb (II)	0.1824	Saah et al. 2024
Magnetic CQDs	Zn (II)	0.4267	Ali et al. 2025
MCQDs	Co (II)	0.2923	This work
	Ni (II)	0.3438	
	Cu (II)	0.4356	
	Zn (II)	0.3676	
	Pb (III)	0.5488	
	Cd (II)	0.3634	
	Cr (III)	0.3726	

where K was the adsorption equilibrium constant, n was the dimensionless exponent of the Freundlich model.

Heavy metal removal

The adsorption equilibrium performance for different heavy metals was presented in Fig. 5a, demonstrating that the MCQDs have the substantial adsorption capacity for various heavy metal ions. Compared with previously reported magnetic carbon quantum dot adsorbents, MCQDs demonstrated superior or comparable adsorption performance (Table 3). MCQDs demonstrated excellent adsorption capabilities for heavy metals, and for elucidating the adsorption mechanism of MCQDs (Fig. 5b), FT-IR and XPS analyses were utilized. Figure 5c illustrated the FT-IR spectra of the sample before and after the adsorption of Cd (II). The peak of MCQDs after Cd (II) adsorption shifted to 3419 cm^{-1}, indicating that the N-H or O-H groups may form interactions with the metal ions (Huang et al. 2019). Besides, for the MCQDs treated with Cd (II) ions, the peaks shifted to 1631 and 1384 cm^{-1}, which was attributed to the links between Cd (II) and the carboxyl group present on MCQDs.

As shown in Fig. 5d, a new peak in the MCQDs was presented, which attributed to Cd (II) from the Cd 3d spectra (Fig. 5e) (Li et al. 2017). For C 1s spectra (Fig. 5f), the C-O and C=O peaks were shifted towards higher binding energy after adsorption, indicating C-O–Cd and C=O-Cd species were present. In addition, the O 1s spectra of samples (Fig. 5g) were composed of three types of peaks, including C=O (513.66 eV), C-OH or C-O-C (530.73 eV), and Fe-O (529.42 eV) (Huang et al. 2019). After the adsorption, the slight increment of binding energy could be attributed to the donation of electron density from oxygen atoms to cadmium ions

(Luo et al. 2021). Meanwhile, the peaks attributed to -NH_2 (404.91 eV) were obviously increased after Cd (II) adsorption in the N 1s spectrum (Fig. 5h). Based on the above findings, the adsorption mechanism of MCQDs was critically dependent on the interactive relationship between metal ions and oxygen-containing groups and amino groups.

Conclusion

In this study, MCQDs were successfully prepared for removing heavy metals by stable combination of CQDs derived from long-root *Eichhornia crassipes* with magnetic substances. Endowed with abundant oxygen-containing and amino groups functional groups on their surface, which provide ample active sites for heavy metal adsorption, MCQDs exhibited excellent adsorption capacity toward various heavy metal ions in aqueous solutions. Furthermore, the material demonstrated satisfactory magnetic recoverability, enhancing practical application in water treatment. These findings not only provided an efficient solution for heavy metal pollution treatment but also successfully promoted the value-added transformation and utilization of waste aquatic biological resources.

Supplementary Information

The online version contains supplementary material available at https://doi.org/10.1186/s40643-026-01064-x.

Supplementary Material 1

Author contributions

Yihong Guo: Conceptualization, Data curation, Methodology, Writing-original draft. Mingxin Cui: Supervision, Funding acquisition, Writing-review & editing. Hongjun Yang: Writing-review & editing. Jun Chen: Formal analysis, Writing-review & editing. Sen Lin: Conceptualization, Funding acquisition, Writing-review & editing.

Funding

This work was supported by the Qinghai University Research Ability Enhancement Project (2025KTST02) and the National Natural Science Foundation of China (92475114).

Data availability

The datasets used and/or analysed during the current study are available from the corresponding author on reasonable request.

Declarations

Ethics approval and consent to participate

Not applicable.

Consent for publication

Not applicable.

Competing interests

The authors declare that they have no competing interests.

Author details

[1]Salt Lake Chemical Engineering Research Complex, Qinghai University, Xining, China
[2]National Engineering Research Center for Integrated Utilization of Salt Lake Resources, East China University of Science and Technology, Shanghai, China
[3]Yunnan Research Institute of Ecological Agriculture, Kunming, China

Received: 7 January 2026 / Revised: 6 March 2026 / Accepted: 12 April 2026
Published online: 28 April 2026

References

Abboud M, Youssef S, Podlecki J et al (2015) Superparamagnetic Fe_3O_4 nanoparticles, synthesis and surface modification. Mater Sci Semiconduct Process 39:641–648. https://doi.org/10.1016/j.mssp.2015.05.035

Ali AO, Aboulrous AA, Mubarak MF et al (2025) Advanced magnetic carbon quantum dots nanocomposite for enhanced removal of zinc and ferric ions from geothermal wastewater: synthesis, characterization, and performance evaluation. ChemistrySelect 10:e05293. https://doi.org/10.1002/slct.202505293

Bao L, Zhang Z-L, Tian Z-Q et al (2011) Electrochemical tuning of luminescent carbon nanodots: from preparation to luminescence mechanism. Adv Mater 23:5801–5806. https://doi.org/10.1002/adma.201102866

Berdimurodov E, Elangovan N, Kumar A et al (2025) Recent advancements in application of carbohydrate-derived carbon quantum dots in analytical chemistry: a comprehensive update. Bioresour Bioprocess 12:121. https://doi.org/10.1186/s40643-025-00953-x

Bilgili MS (2006) Adsorption of 4-chlorophenol from aqueous solutions by xad-4 resin: isotherm, kinetic, and thermodynamic analysis. J Hazard Mater 137:157–164. https://doi.org/10.1016/j.jhazmat.2006.01.005

Cao F, Lian C, Yu J et al (2019) Study on the adsorption performance and competitive mechanism for heavy metal contaminants removal using novel multi-pore activated carbons derived from recyclable long-root *Eichhornia crassipes*. Bioresour Technol 276:211–218. https://doi.org/10.1016/j.biortech.2019.01.007

Chen D, Li Y, Zhang J et al (2012) Magnetic Fe_3O_4/ZnCr-layered double hydroxide composite with enhanced adsorption and photocatalytic activity. Chem Eng J 185–186:120–126. https://doi.org/10.1016/j.cej.2012.01.059

Chen J, Lin S, Yu J (2020) Quantitative effects of Fe3O4 nanoparticle content on Li^+ adsorption and magnetic recovery performances of magnetic lithium-aluminum layered double hydroxides in ultrahigh Mg/Li ratio brines. J Hazard Mater 388:122101. https://doi.org/10.1016/j.jhazmat.2020.122101

Chen J, Lin S, Yu J (2021a) High-selective cyclic adsorption and magnetic recovery performance of magnetic lithium-aluminum layered double hydroxides (MLDHs) in extracting Li^+ from ultrahigh Mg/Li ratio brines. Sep Purif Technol 255:117710. https://doi.org/10.1016/j.seppur.2020.117710

Chen M, Fang Z, Xu L et al (2021b) Enhancement of photo-driven biomethanation under visible light by nano-engineering of Rhodopseudomonas palustris. Bioresources Bioprocess 8:30

Chen Q, Rong S, Cen Y et al (2021c) A facile fluorescent sensor based on carbon dots and Fe3O4 nanoplates for the detection of hyaluronidase activity. Sens Actuators B 346:130434. https://doi.org/10.1016/j.snb.2021.130434

Cheung WH, Szeto YS, McKay G (2007) Intraparticle diffusion processes during acid dye adsorption onto chitosan. Bioresour Technol 98:2897–2904. https://doi.org/10.1016/j.biortech.2006.09.045

Đorđević L (2022) A multifunctional chemical toolbox to engineer carbon dots for biomedical and energy applications. Nat Nanotechnol 17:112–130. https://doi.org/10.1038/s41565-021-01051-7

Durairaj A, Maruthapandi M, Luong JHT et al (2022) Enhanced UV protection, heavy metal detection, and antibacterial properties of biomass-derived carbon dots coated on protective fabrics. ACS Appl Bio Mater 5:5790–5799. https://doi.org/10.1021/acsabm.2c00798

El Ghacham S, Aoulad El Hadj Ali Y, Hejji L et al (2025) Efficiency of magnetite decorated with carbon quantum dot nanocomposites for the adsorptive removal of methylene blue from wastewater: kinetic and modeling studies. J Mol Liq 424:127128. https://doi.org/10.1016/j.molliq.2025.127128

Huang S, Jiang S, Pang H et al (2019) Dual functional nanocomposites of magnetic MnFe2O4 and fluorescent carbon dots for efficient U(VI) removal. Chem Eng J 368:941–950. https://doi.org/10.1016/j.cej.2019.03.015

Jia Z, Hu J, Lu P, Wang Y (2024) Carbon quantum dots from carbohydrate-rich residue of birch obtained following lignin-first strategy. Bioresour Technol 408:131206. https://doi.org/10.1016/j.biortech.2024.131206

Kunnath Parambil NS, Dasan A, Premkumar AT et al (2025) Blue luminescent carbon quantum dots derived from diverse banana peels for selective sensing of Fe(III) ions. Sens Int 6:100301. https://doi.org/10.1016/j.sintl.2024.100301

Li R, Liang W, Li M et al (2017) Removal of Cd(II) and Cr(VI) ions by highly cross-linked thiocarbohydrazide-chitosan gel. Int J Biol Macromol 104:1072–1081. https://doi.org/10.1016/j.ijbiomac.2017.07.005

Lima EC, Hosseini-Bandegharaei A, Moreno-Piraján JC, Anastopoulos I (2019) A critical review of the estimation of the thermodynamic parameters on adsorption equilibria. Wrong use of equilibrium constant in the Van't Hoof equation for calculation of thermodynamic parameters of adsorption. J Mol Liq 273:425–434. https://doi.org/10.1016/j.molliq.2018.10.048

Lin S, Wang G, Na Z et al (2012) Long-root *Eichhornia crassipes* as a biodegradable adsorbent for aqueous As(III) and As(V). Chem Eng J 183:365–371. https://doi.org/10.1016/j.cej.2012.01.013

Lin S, Yang H, Na Z, Lin K (2018) A novel biodegradable arsenic adsorbent by immobilization of iron oxyhydroxide (FeOOH) on the root powder of long-root *Eichhornia crassipes*. Chemosphere 192:258–266. https://doi.org/10.1016/j.chemosphere.2017.10.163

Lin S, Huang W, Yang H et al (2020) Recycling application of waste long-root *Eichhornia crassipes* in the heavy metal removal using oxidized biochar derived as adsorbents. Bioresour Technol 314:123749. https://doi.org/10.1016/j.biortech.2020.123749

Lin S, Guo Y, Zhou L, Yang H (2022) Quantitative effects of surface oxidation on biochar derived from long-root *Eichhornia crassipes* plants as Cd^{2+} adsorbent. Bioresour Technol Rep 17:100937. https://doi.org/10.1016/j.biteb.2021.100937

Liu L, Hu S, Shen G et al (2018) Adsorption dynamics and mechanism of aqueous sulfachloropyridazine and analogues using the root powder of recyclable long-root *Eichhornia crassipes*. Chemosphere 196:409–417. https://doi.org/10.1016/j.chemosphere.2018.01.003

Liu L, Sim SF, Lin S et al (2021) Integrated structural and chemical analyses for HCl-supported hydrochar and their adsorption mechanisms for aqueous sulfachloropyridazine removal. J Hazard Mater 417:126009. https://doi.org/10.1016/j.jhazmat.2021.126009

Luo Q, Huang X, Luo Y et al (2021) Fluorescent chitosan-based hydrogel incorporating titanate and cellulose nanofibers modified with carbon dots for adsorption and detection of Cr(VI). Chem Eng J 407:127050. https://doi.org/10.1016/j.cej.2020.127050

Mahesh S, Lekshmi CL, Renuka KD, Joseph K (2016) Simple and cost-effective synthesis of fluorescent graphene quantum dots from honey: application as stable security ink and white-light emission. Part Part Syst Charact 33:70–74. https://doi.org/10.1002/ppsc.201500103

Mashkani M, Mehdinia A, Jabbari A et al (2018) Preconcentration and extraction of lead ions in vegetable and water samples by N-doped carbon quantum dot conjugated with Fe3O4 as a green and facial adsorbent. Food Chem 239:1019–1026. https://doi.org/10.1016/j.foodchem.2017.07.042

Nguyen TN, Le PA, Phung VBT (2022) Facile green synthesis of carbon quantum dots and biomass-derived activated carbon from banana peels: synthesis and investigation. Biomass Convers Bioref 12:2407–2416. https://doi.org/10.1007/s13399-020-00839-2

Pourshojaei Y, Nasiri A, Asadollahzadeh H et al (2021) Developing a magnetic nanocomposite adsorbent based on carbon quantum dots prepared from pomegranate peel for the removal of Pb(II) and Cd(II) ions from aqueous solution. Anal Methods Environ Chem J 4:33–46. https://doi.org/10.24200/amecj.v4.i03.149

Saah F, Nagpal G, Gbawoquiyq F, Chaudhary R (2024) Groundnut shell carbon quantum dot magnetic iron oxide nanocomposite (GSCQD-$FeFe_2O_4$) for lead removal from water. Zas Mater 65:440–451. https://doi.org/10.62638/ZasMat1185

Tian L, Ghosh D, Chen W et al (2009) Nanosized carbon particles from natural gas soot. Chem Mater 21:2803–2809. https://doi.org/10.1021/cm900709w

Wang Y, Hu A (2014) Carbon quantum dots: synthesis, properties and applications. J Mater Chem C 2:6921. https://doi.org/10.1039/C4TC00988F

Wang L, Li W, Wu B et al (2016) Facile synthesis of fluorescent graphene quantum dots from coffee grounds for bioimaging and sensing. Chem Eng J 300:75–82. https://doi.org/10.1016/j.cej.2016.04.123

Yang S-T, Cao L, Luo PG et al (2009) Carbon dots for optical imaging in vivo. J Am Chem Soc 131:11308–11309. https://doi.org/10.1021/ja904843x

Zhu S, Meng Q, Wang L et al (2013) Highly photoluminescent carbon dots for multicolor patterning, sensors, and bioimaging. Angew Chem 125:4045–4049. https://doi.org/10.1002/ange.201300519

Publisher's note

Springer Nature remains neutral with regard to jurisdictional claims in published maps and institutional affiliations.